Microsc. Microanal. Page 1 of 9
doi:10.1017/S1431927612014419

Microscopy AND Microanalysis

A (S)TEM Gas Cell Holder with Localized Laser Heating for *In Situ* Experiments

Shareghe Mehraeen,[1,*] Joseph T. McKeown,[2,*] Pushkarraj V. Deshmukh,[3] James E. Evans,[1,4] Patricia Abellan,[4] Pinghong Xu,[5] Bryan W. Reed,[2] Mitra L. Taheri,[6] Paul E. Fischione,[3] and Nigel D. Browning[1,4,5]

[1]*Department of Molecular and Cellular Biology, University of California, Davis, CA 95616, USA*
[2]*Condensed Matter and Materials Division, Lawrence Livermore National Laboratory, Livermore, CA 94550, USA*
[3]*E.A. Fischione Instruments, Inc., Export, PA 15632, USA*
[4]*Chemical and Materials Science Division, Pacific Northwest National Laboratory, Richland, WA 99352, USA*
[5]*Department of Chemical Engineering and Materials Science, University of California, Davis, CA 95616, USA*
[6]*Department of Materials Science & Engineering, Drexel University, Philadelphia, PA 19104, USA*

Abstract: The advent of aberration correction for transmission electron microscopy has transformed atomic resolution imaging into a nearly routine technique for structural analysis. Now an emerging frontier in electron microscopy is the development of *in situ* capabilities to observe reactions at atomic resolution in real time and within realistic environments. Here we present a new *in situ* gas cell holder that is designed for compatibility with a wide variety of sample type (i.e., dimpled 3-mm discs, standard mesh grids, various types of focused ion beam lamellae attached to half grids). Its capabilities include localized heating and precise control of the gas pressure and composition while simultaneously allowing atomic resolution imaging at ambient pressure. The results show that 0.25-nm lattice fringes are directly visible for nanoparticles imaged at ambient pressure with gas path lengths up to 20 μm. Additionally, we quantitatively demonstrate that while the attainable contrast and resolution decrease with increasing pressure and gas path length, resolutions better than 0.2 nm should be accessible at ambient pressure with gas path lengths less than the 15 μm utilized for these experiments.

Key words: *in situ* gas holder, STEM, environmental microscopy, *in situ* microscopy, aberration correction, laser heating

Introduction

The ability to study gas-solid interactions with atomic resolution and ambient pressures in the transmission electron microscope (TEM) promises new insights into the growth, properties, and functionality of nanomaterials. Heterogeneous catalysis is a particular application in which the structure, morphology, and chemistry of nanoparticles are dynamic and greatly depend on the gas environment and temperature (Boyes & Gai, 1997; Hansen et al., 2002; Giorgio et al., 2006; Gai et al., 2007; Ueda et al., 2008; Wang et al., 2009; Chang et al., 2010). Unfortunately, conventional high-resolution TEM of catalysis is extremely challenging because both ambient pressure and elevated temperature can adversely affect imaging conditions. This is further complicated by the fact that normal TEM imaging is performed under a high vacuum (1.5×10^{-7} Torr) to prevent unwanted scattering from gases. Therefore, to enable *in situ* experiments within the column of an electron microscope, a localized gas environmental chamber with controllable gas pressure, composition, and temperature is crucial. Such conditions can be obtained using an environmental cell built around the specimen.

The original designs for environmental cells have been around for over 70 years (Marton, 1935) and are produced by either incorporating differentially pumped apertures that separate the specimen from the high vacuum of the TEM column (Baker & Harris, 1972; Butler & Hale, 1981; Lee et al., 1991; Boyes & Gai, 1997; Robertson & Teter, 1998; Sharma & Weiss, 1998; Sharma, 2001, 2005; Zhang et al., 2005) or windowed-cell designs that confine the gas within the specimen holder using electron-transparent membranes (Heide, 1962; Butler & Hale, 1981; Parkinson, 1989; Daulton et al., 2001; Konishi et al., 2003; Komatsu & Mori, 2005; Giorgio et al., 2006; Creemer et al., 2008). Atomic-resolution images in gaseous environments have been obtained with both techniques (Parkinson, 1989; Boyes & Gai, 1997; Sharma & Weiss, 1998; Hansen et al., 2002; Helveg et al., 2004; Yaguchi et al., 2011; Allard et al., 2012). Environmental transmission electron microscopes (ETEMs) that incorporate differentially pumped apertures are generally limited to pressures of 15–20 Torr, but they permit imaging a standard TEM sample. A windowed-cell approach produces a much thinner layer of gas (or fluid) than a differentially pumped ETEM and can examine samples at pressures greater than 50 Torr (Butler & Hale, 1981; Creemer et al., 2008; Yaguchi et al., 2011; Allard et al., 2012). However, the additional electron scattering due to the window membranes can decrease the attainable contrast and resolution. Recently, atomic-resolution imaging in a liquid environment was acquired at ambient pressure using a windowed-cell *in situ* liquid holder with fluid path lengths

Received September 17, 2012; accepted December 5, 2012
*Corresponding author. E-mail: smehraeen@gmail.com, mckeown3@llnl.gov

of 200–400 nm (Evans et al., 2011). Unfortunately, such a thin path length for gaseous experiments would only be amenable to nanoparticle research and not conventional dimpled and ion milled specimens.

While atomic-resolution *in situ* imaging in gas cell holders has been previously demonstrated using a windowed-cell approach at atmospheric pressure and temperatures up to 500°C (Creemer et al., 2008; Allard et al., 2012), many reactions, including those involving catalysts, require a greater temperature range. Additionally, the micromachined devices used in previous designs (Creemer et al., 2008; Allard et al., 2012) heat the entire window surface and simultaneously react every nanoparticle. A direct heating source that is smaller than the windowed area and translatable across the surface would allow multiple experiments to be imaged under equivalent pressure and temperature conditions but at separate times to improve reproducibility. Possibilities for such localized heating could incorporate a partitioned micromachined device or focused laser. A new environmental-cell design using windowed cells with a variable gas path length (GPL) is therefore critically needed to permit *in situ* observations of any type of sample at ambient pressure and elevated temperature in a manner that allows atomic resolution and statistical measurements through targeted heating and imaging.

Atomic-scale imaging of catalysts and other nanoparticles would also benefit from *in situ* aberration-corrected high-angle annular dark-field scanning TEM (HAADF-STEM) imaging (Nellist et al., 2004). This imaging mode can provide directly interpretable atomic-scale images of catalyst nanoparticles at the required pressures and temperatures, as recently demonstrated (de Jonge et al., 2010; Allard et al., 2012). The use of an aberration-corrected STEM can significantly improve the resolution by producing a smaller electron probe ($<$1 Å in some instances) relative to an uncorrected STEM, as the dark-field resolution is largely determined by the probe diameter. HAADF-STEM imaging is produced from incoherent, Rutherford-like scattering of electrons to high angles by the atomic nuclei of the specimen. The intensity (contrast) in the images is related to both the density and thickness (mass-thickness contrast) and the atomic number of the species responsible for scattering (typically referred to as Z-contrast imaging), generating images that reveal chemical information as well as structural information without potentially unwanted diffraction contrast (Crewe et al., 1969, 1970; Pennycook, 1989). This makes HAADF-STEM imaging ideal for catalysis studies in which small particles or clusters of heavy atoms sit on a substrate, and it is necessary to differentiate chemically inhomogeneous structures at small spatial scales (Treacy et al., 1978; Pennycook, 1981; Howie et al., 1982; Pennycook et al., 1983).

Here, we demonstrate the capabilities of a new *in situ* holder capable of precisely controlling gas composition and pressure. The new holder has the ability to image any type of sample [i.e., dimpled 3-mm discs, standard mesh grids, various types of focused ion beam (FIB) lamellae attached to half grids] because the GPL is adjustable between 0 and 250 μm and enables access to experiments at higher temperatures than previous designs by incorporation of localized specimen heating using a translatable fiber-based laser. In this article, we present atomic-resolution images obtained with aberration-corrected HAADF-STEM from two distinct experiments using nanoparticle specimens (TiO_2 and PbO). The images were acquired at ambient temperature and a range of pressures up to 800 Torr. Finally, we evaluate the effect of gas pressure on attainable resolution.

Materials and Methods

Nanoparticle Preparation

PbO nanoparticles were grown by first forming lead sulfide nanoparticles in solution (Evans et al., 2011) followed by deposition on the window surface and oxidation at room temperature and atmosphere (Zingg & Hercules, 1978). The TiO_2 nanopowder [Sigma Aldrich®, $\geq$99.5% pure titanium (IV) oxide, 25 nm; Sigma-Aldrich, St. Louis, MO, USA] and Zn nanoparticles (Skyspring Nanomaterials, 99.9% zinc, 80–100 nm; Skyspring Nanomaterials, Houston, TX, USA) were used as purchased and deposited directly on the window surface as a dry powder prior to imaging. In the case of the Zn nanoparticles, the exposure to air during loading of the holder resulted in the formation of a zinc oxide shell surrounding the Zn core. For the experiments described here, nanoparticles were placed directly on the inner side of the upper membrane (entrance window with respect to the scanning electron probe) of the environmental cell (e-cell) to minimize probe broadening prior to scattering by the specimen (Mkhoyan et al., 2008).

In Situ Holder Design

The design (Deshmukh et al., 2012) of the *in situ* environmental heating holder (E.A. Fischione Instruments, Inc., Export, PA, USA) employed in these studies incorporates a windowed e-cell with a total height of 2 mm. Figure 1 shows schematics and photos of the holder design, including an illustration of the loading procedure for the e-cell. A pair of 15-nm-thick amorphous silicon nitride windows (Ted Pella, Inc., Redding, CA, USA) created the electron-transparent reaction chamber as shown in Figure 1B. The e-cell is designed to accept a standard 3-mm-diameter TEM specimen, which allows for dimpled 3-mm discs, particles deposited on grids, various types of FIB lamellae attached to half-grids, etc. A modular, adaptive design allows for a variation in the spacer height and GPL to accommodate various sample thicknesses up to 250 μm. The modular spacers consist of 15-μm-thick titanium discs with an outer diameter of 3 mm and an inner diameter of 1 mm to provide a gap between the two silicon nitride membranes for gas flow in and out of the e-cell without obscuring the viewable area. Gas flow in and out of the e-cell is accomplished *via* inlet and outlet tubes that run through the length of the holder shaft to the e-cell at the tip of the holder, as illustrated in Figure 1C.

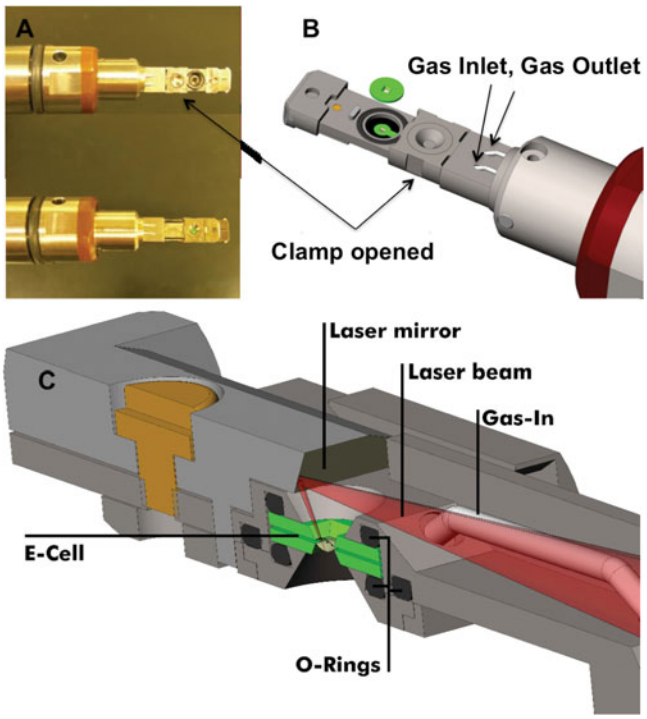

Figure 1. Overview of environmental gas-cell holder design. **A:** The tip of the *in situ* holder before mounting the windows (top) and after inserting the windows and securing the clamp to seal the e-cell (bottom). **B:** Loading the e-cell with the nitride windows and spacer. **C:** Side-view cross section of the holder showing the loaded e-cell, gas inlet tube that runs the length of the holder shaft, and localized laser heating with the position of the mirror above the e-cell.

The holder also incorporates a built-in laser optics assembly to focus an infrared laser onto the specimen for localized heating experiments. The laser enters the end of the holder via a fiber optic cable and is focused onto the sample using a 60° titanium mirror with 5-nm gold plating, as shown in Figure 1C. The optics are adjustable to yield a spot size on the sample between 30 and 300 μm and translatable along the sample plane x- and y-axes. The laser can also be pulsed. The small heated zone/laser pulsing can help minimize the negative effects of radiation, convection, and conduction in the e-cell. Ongoing studies are focused on temperature calibration using the laser, as this will be specimen specific. The laser optics can also be easily exchanged to incorporate a wide range of wavelengths for specific applications, such as photocatalysis.

Figure 2 shows a schematic of the complete gas-flow assembly. This design has the provision of flowing up to four different gases simultaneously through the cell. The gas flow is controlled accurately using mass flow controllers and monitored with pressure regulators installed on all four gas lines. The gases initially flow into a mixing chamber external to the TEM holder, and from there the gas mixture is circulated into the specimen chamber of the holder through the inlet port. Nylon gas tubes are used for the flow of gases from the external gas-flow assembly to the holder and from the holder to the exhaust. Apart from having a high chemical resistance, the stiffness properties of nylon help to dampen the vibrations originating from the gas assembly. Nylon connectors are further incorporated at the inlet and outlet port of the holder, which helps to isolate any residual

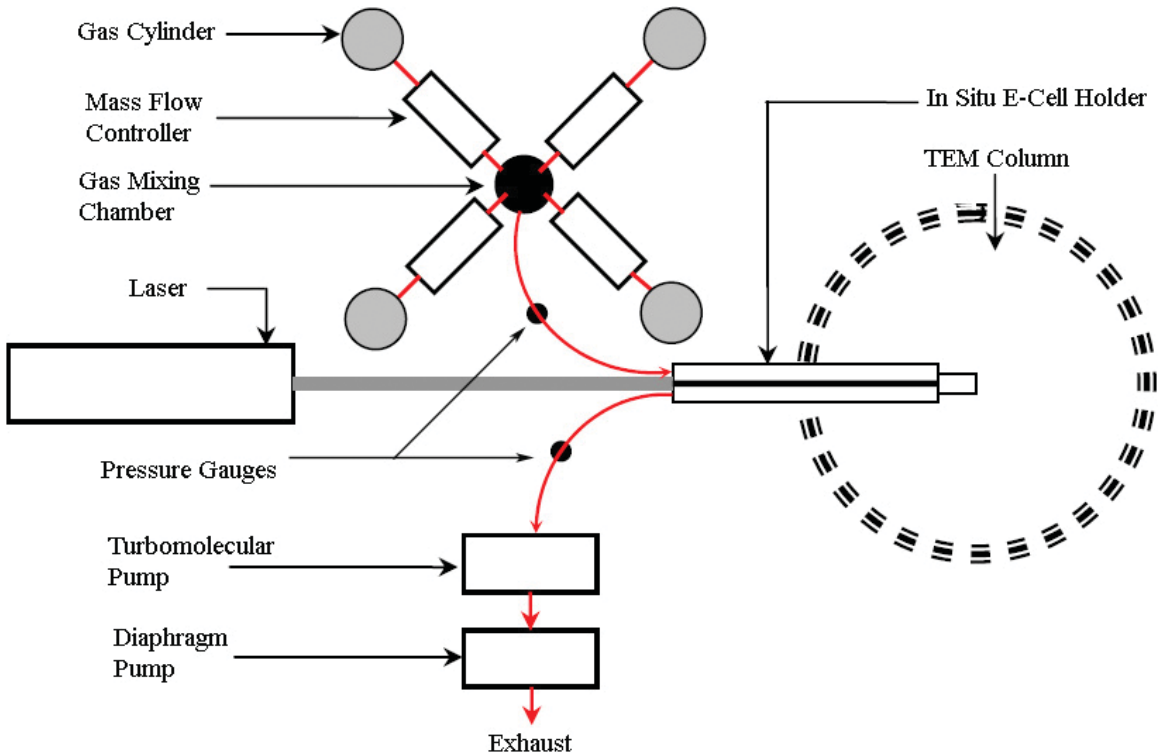

Figure 2. Schematic view of the complete gas flow assembly.

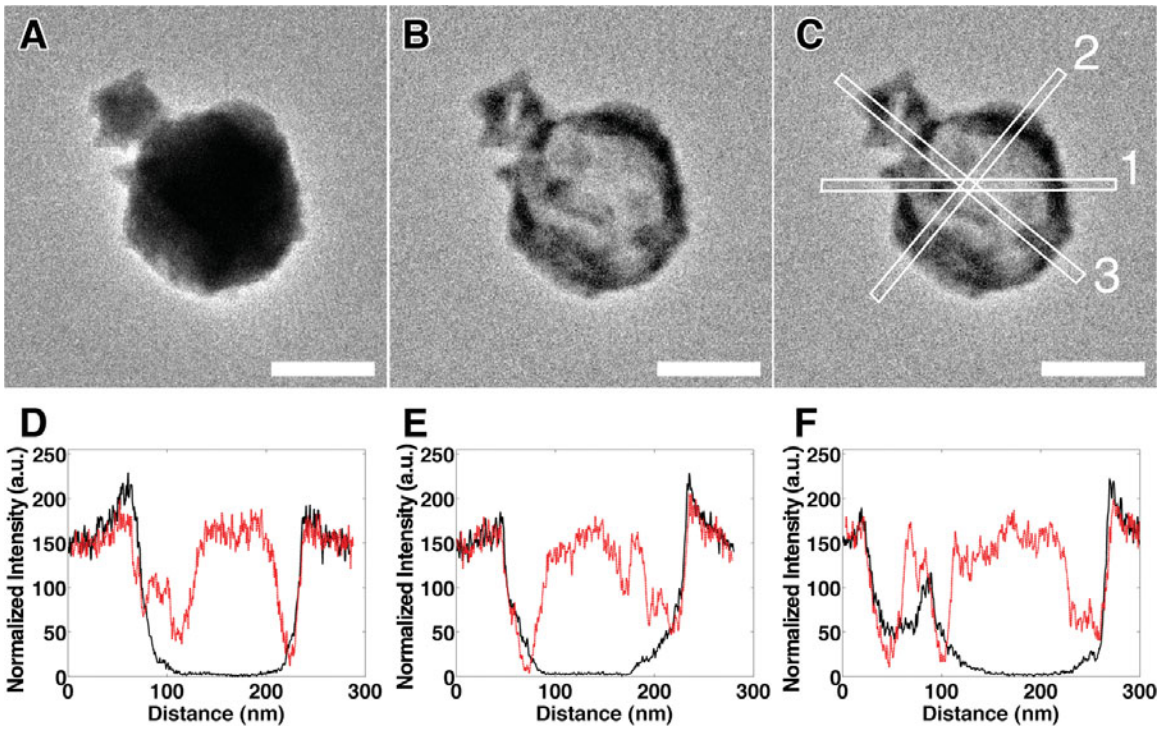

Figure 3. Generation of hollow zinc oxide nanoparticle using localized infrared laser heating. **A:** Zn/ZnO core-shell nanoparticle imaged at room temperature. **B:** Same particle as panel **A** following exposure to a 200-μm-diameter continuous 1085-nm laser for 15 s with a power density of 4.9×107 W/m^2. Only the hollow ZnO shell remains. The scale bar is equivalent for both panels and represents 100 nm. **C:** Illustration showing the equivalent line scan regions for the particles shown in panels **A** and **B**. Line scans 1–3 correspond to panels **D–F**, respectively. Black line in the graphs represents the intensity before the heating and red line shows after the heating. All line scans depict the 20-pixel-wide integrated profile before and after heating.

vibrations. Pressure gauges at the inlet and outlet ports of the holder are used to determine the average steady-state pressure within the e-cell. Simultaneous pumping of the e-cell with an external two-stage diaphragm and turbomolecular pump and/or regulating the mass flow rate of the gases can accurately vary the pressure inside the e-cell. All flow regulations are computer controlled using a LabVIEW^{TM} interface.

Scanning Transmission Electron Microscopy and *In Situ* Experiments

HAADF-STEM imaging with the *in situ* holder was performed in an aberration-corrected JEOL JEM-2100F/Cs (JEOL Ltd., Tokyo, Japan) operating at 200 keV using a probe current of ~72 pA and a dwell time of 15 μs/pixel. TEM imaging was performed in an aberration-corrected JEOL JEM-2200F, also operated at 200 keV. All *in situ* images were recorded in O_2 gas with >99.5% purity, as this provides a means of removing hydrocarbon contamination that may develop during experiments (Heide, 1962). For the heating experiment, a 1085-nm laser (total power output of 8.5 W) was operated at 18% power with a sample plane spot size of 200 μm providing a power density at the sample of 4.9×10^7 W/m^2.

Insertion of the gas cell holder into the microscope prepump chamber proceeds simultaneously with starting the assembly pumps connected to the e-cell to maintain a low pressure differential. The silicon nitride membranes are sensitive to the applied strain rate, so it is essential to ramp the pressure gradually to minimize the pressure shock. Multiple failures of silicon nitride membranes occurred within the prepump chamber prior to experiments (evident on the installed pressure gauges). However, after replacement and successful insertion into the TEM, we achieved a 100% success rate with respect to membrane failure (no membranes ruptured while in the microscope column). The rupture of the silicon nitride membranes was attributed to the sudden drop in pressure around the e-cell. In the future, it is envisioned to control the pumping speed at which the prepump chamber is evacuated and the utilization of custom nitride membranes with a greater resistance to pressure changes. Once inside the microscope and prior to imaging experiments, the e-cell was evacuated to ~10 Torr using the external pumps connected to the gas outlet line shown in Figure 1. The pumps were then stopped and O_2 gas was introduced into the e-cell using the mass flow controllers until the desired steady-state pressure was achieved within the e-cell (i.e., when the pressures on both the inlet and outlet gauges were equal and static).

Results and Discussion

Figure 3 shows bright-field TEM images of hollow zinc oxide nanoparticle generation from a core-shell zinc/zinc

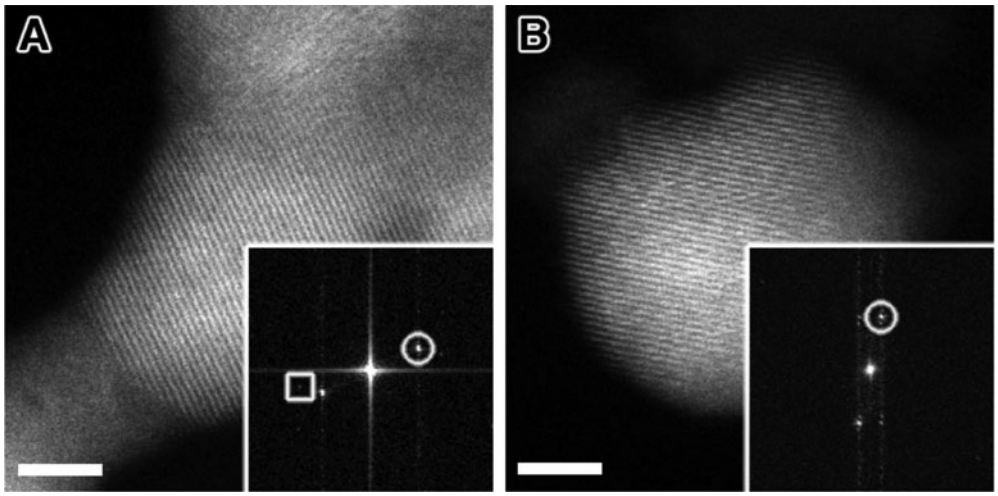

Figure 4. Atomic-scale resolution under gas flow. PbO nanoparticles showing atomic lattice fringes at (**A**) 20-Torr and (**B**) 800-Torr O_2 gas. FT insets show 0.25-nm lattice fringes (white circles) corresponding to (002) lattice planes and the 0.18-nm lattice fringes (white square). Scale bars represent 3 nm.

oxide (Zn/ZnO) nanoparticle following infrared heating. Power spectra of the amorphous SiN membrane to which the nanoparticles are attached show that the images were acquired at the same focus, indicating the contrast change is not due to defocus effects. At a laser power setting of 18% and a spot size of 200 μm (power density of 4.9×10^7 W/m^2), the solid zinc core disappears leaving behind a zinc oxide shell as a hollow nanoparticle. Diffraction patterns of nanoparticles before heating confirmed the presence of a Zn/ZnO core shell particle while diffraction patterns of the same particles after heating only showed evidence of a ZnO shell. Similar results were achieved during previously published *ex situ* laser heating experiments (Niu et al., 2010), where hollow ZnO nanoparticles were formed following selective-laser vaporization of Zn/ZnO core shell nanoparticles. The vaporization of the solid core occurs when the nanoparticle is heated (with a laser photon energy below the band gap of the shell material) to a temperature above the core material boiling point but below the shell material melting point. For the Zn/ZnO nanoparticle shown in Figure 3, this corresponds to a temperature above 907°C but below 1975°C (Niu et al., 2010). To verify that the ZnO shell did not expand during this experiment while the Zn core disappeared, we included line profiles for equivalent regions of the nanoparticle before and after heating (Figs. 3C–3F). Since we systematically increased the laser temperature to achieve these results, we are confident that we are above 907°C, but we are not sure of the deviation above this value. A more detailed analysis using multiple samples (of similar size and shape) and data points will be needed to fully calibrate a plot for laser power versus sample temperature. Based on these results, it would be theoretically possible to achieve a local sample temperature greater than 10,000°C with this holder if the power density was increased to 50% and the spot size decreased to 100 μm (assuming a linear effect and a similar sample absorption rate of 40%) (Bergström et al., 2007). However, a maximum operating value of 2000°C is more realistic for this *in situ* gas holder. This temperature limit would avoid thermal radiation from the sample compromising the integrity of the silicon nitride membrane and gold plating on the mirror. Although the higher temperature capabilities of the holder are the focus of a separate article, the possibility of achieving localized sample temperatures up to 2000°C will permit imaging of many high-temperature catalyst systems currently not amenable to *in situ* analysis.

As a first test specimen for verifying the resolution achievable with HAADF-STEM and the new *in situ* gas holder under atmospheric conditions, we imaged PbO nanoparticles directly attached on the inner side of the upper membrane. Figure 4 shows raw images of PbO recorded at 20 and 800 Torr (>1 atm) along with respective direct Fourier transforms (FT). Lattice fringes at 0.25 nm are visible in the images of PbO nanoparticles at all applied pressures up to 800 Torr (average steady state). However, while we detected 0.18-nm fringes while imaging particles at 20 Torr, none of the particles imaged at 800 Torr depicted fringes beyond 0.2 nm. This could of course be due to the orientation of the nanoparticles during imaging, or it could be due to an adverse effect for resolution dependent on gas pressure, path length, and/or membrane thickness.

Any loss of resolution due to increasing the gas pressure to 800 Torr can be explained by plural scattering from a combined effect of the silicon nitride membranes and gas molecules. Unlike standard imaging where the sample is exposed to the vacuum of the microscope, *in situ* e-cell imaging (both gas and liquid environments) involves extra material density surrounding the sample of interest, which causes plural scattering and can degrade image contrast and resolution. Additionally, this effect worsens as the pressure increases due to outward membrane bulging that results in a larger GPL. However, the magnitude of resolution loss is dependent on where the sample is located relative to the upper membrane. With the sample adhered to the opposite

(bottom) window, the scanned probe is broadened significantly due to scattering caused by interaction of the electron beam with the upper window and the density of gas molecules prior to surveying the sample (Mkhoyan et al., 2008). Since the resolution in HAADF-STEM is dependent on the probe size, this type of broadening directly limits the attainable resolution. During these experiments we were unable to detect any lattice fringes for nanoparticles on the bottom window. On the other hand, when the particles are attached to the upper membrane, the scattering from the gas density occurs after the electrons have already interacted with the specimen and decreases the signal-to-background ratio, as some electrons that would have hit the HAADF detector will be randomly scattered away from it and vice versa. Thus, there may be some critical pressure, GPL, and/or density beyond which atomic lattice fringes for a given resolution will no longer be observed as the noise effectively blurs the lattice fringes.

For our experiments, the initial GPL was nominally set with a single 15-μm titanium spacer inserted between the upper and the lower silicon frames. When the e-cell was pressurized, the silicon nitride membranes bulged due to the pressure differential between the e-cell and vacuum of the microscope column, and the bulging was measured experimentally by calculating the change in eucentric height position of each membrane as the pressure inside the e-cell increased. While the GPL at the edge of the windowed area matched the nominal spacing of 15 μm, the middle of the window bulged to a GPL of $\sim$50 μm at 760 Torr. Using the approach of Creemer et al. (2010), we calculated the atomic density projected along the path of the electron beam through the gas by integrating the molecular density through the thickness of the environmental cell (there will be contributions from both the window membranes and the gas). For O_2 gas at 760 Torr and 300 K with a 50-μm GPL, this gives a projected density of $\sim 2.5 \times 10^3$ atoms/nm^2 due to the gas molecules only. This projected gas density matches the density previously obtained both in a nanoreactor with H_2 gas at $\sim$750 Torr (34-μm GPL and 0.18-nm resolution) and in an ETEM with N_2 gas at $\sim$4 Torr (5-mm GPL and 0.14-nm resolution) (Hansen et al., 2006). Interestingly, atomic resolution was not obtained in the present experiments when the GPL was 50 μm for particles on the upper window. Instead, a critical path length of less than 20 μm was required to observe lattice fringes at 760 Torr and above. Taking into account the contribution from the 15-nm-thick nitride membranes, this corresponds to a critical projected atomic density of $\sim 7 \times 10^3$ atoms/nm^2 ($\sim 1 \times 10^3$ atoms/nm^2 are due to the gas molecules). Since each silicon nitride membrane contributes 3×10^3 atoms/nm^2 in the projected atomic density, scattering from the membranes is currently much stronger than the scattering from the gas molecules. As a result, using thinner membranes would likely permit even higher resolution imaging conditions than presented here; however, a simultaneous decrease in window areas will be required to maintain sufficient mechanical resistance to the differential pressure experienced by the e-cell during loading into the microscope.

To verify these results and test the versatility of combining the *in situ* holder with HAADF-STEM for imaging nanoparticles composed of lower atomic number elements, a titanium (IV) oxide (TiO_2) nanopowder with an average particle size of $\sim$25 nm was also imaged. Figure 5 shows atomic-resolution HAADF-STEM images of TiO_2 nanoparticles at four pressures ranging from the vacuum of the microscope column ($\sim 10^{-7}$ Torr) to 760 Torr. All images were recorded at a GPL of $\sim$20 μm. To quantify the resolution loss as a function of pressure, we analyzed line profiles and Bragg spot intensities corresponding to the 0.25-nm lattice fringes from the nanoparticles shown in Figures 5A–5D. Since the membrane thickness used for these images were identical, the images were shifted to an equivalent average pixel value for the amorphous SiN background prior to calculating the line profiles. This constant adjustment of pixel values generated a relative reference value from which the effect of pressure on resolution could be assessed. As seen in Figure 5E, the average signal levels of the particles and background were similar for both the 40- and 760-Torr images. However, the peak-to-valley height for the 0.25-nm lattice fringes at 760 Torr was roughly 33% of the height at 40 Torr. The decrease in fringe visibility with increasing pressure was validated by a second measurement of Bragg spot intensity quotient (IQ) values. To calculate the IQ values, direct FTs of the images were performed and the central peak intensity of each Bragg spot was compared to the average intensity of background pixels. To ensure the background pixels were representative and did not include above-average intensity due to a broadened spot, a radius of 10 pixels from the central peak was used to calculate the average background value (excluding all values within 9 pixels of the central peak). Figure 5F depicts a plot of the IQ values normalized to the IQ value calculated at 40 Torr. The plot indicates a decrease of spot intensity at 760 Torr to 72% of the intensity at 40 Torr. It is important to note that the line profile analysis is an absolute measure while the IQ analysis is a relative measure of contrast. The IQ analysis has been used for over 25 years in the biological TEM community where it was developed to evaluate images with low signal-to-noise levels (Henderson et al., 1986). Although the doses used here were higher than the typical low-dose images of biological TEM, the IQ analysis provided a convenient mechanism for qualitatively comparing the different imaging conditions due to varying pressure. Bragg spots can be detected in the power spectrum of an image even when the particle contrast is nearly zero. Thus, despite the discrepancy in magnitude between the two measurements appearing large, both analysis methods support a significant loss of contrast and resolution as a function of pressure. The observation that the 0.18-nm fringes were absent in images acquired at ambient pressure (while the 0.25-nm fringes remained visible) suggests that plural scattering limited the resolution to around 0.2 nm for the microscope and holder assembly conditions utilized during

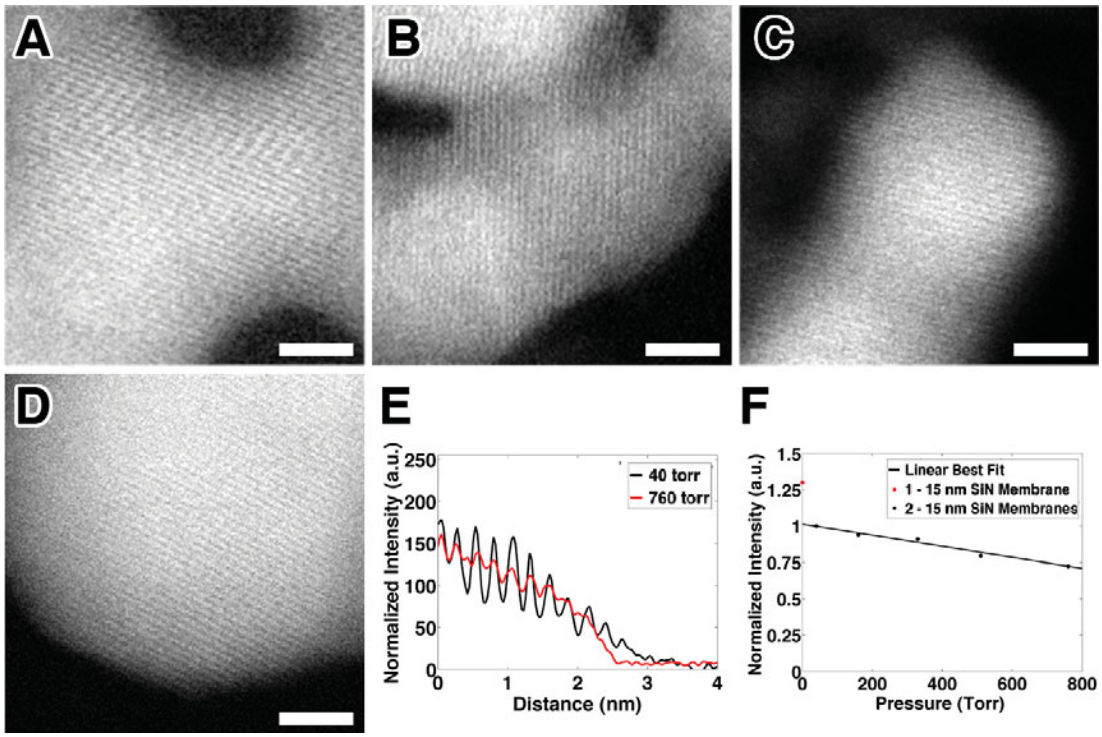

Figure 5. HAADF-STEM images showing lattice fringes for TiO_2 nanoparticles attached to silicon nitride membranes. **A–D:** Nanoparticles deposited between two 15-nm silicon nitride membranes inside the *in situ* environmental holder at 40-, 163-, 330-, and 760-Torr O_2 gas, respectively. Scale bars represent 3 nm. **E:** Plot showing line profiles for the nanoparticles depicted in panels **A** and **D** perpendicular to the 0.25-nm lattice fringes. **F:** Plot showing normalized IQ value of the 0.25-nm spots for six different gas pressures. The black circles indicate IQ values from particles between two membranes at pressures between 40 and 760 Torr. The red circle indicates the IQ value for a nanoparticle atop a single membrane and exposed to the high vacuum of the microscope ($\sim 10^{-7}$ Torr) for reference.

these experiments. Since the GPL was held approximately constant for all images in Figure 5, the resolution loss was due to the change in pressure. However, since both pressure and GPL affect the total number of gas molecules that reside in the path of the electron beam and cause plural scattering, the use of a thinner nominal path length than the 15-μm spacer used here may permit imaging on the 1-Å scale for future experiments.

Summary

The results presented here demonstrate that this new combined gas cell/heating holder is capable of localized heating and obtaining atomic-resolution images from nanoparticles at technologically relevant pressures greater than 760 Torr. The new holder design bypasses limitations imposed by sample size and field of view. Optimization of the parameters required for atomic-resolution STEM imaging in ambient pressures involved overcoming several multifaceted challenges in design, engineering, and experimental planning such as specimen drift, carbon contamination, and blurring factor of the windows. The first results of these efforts are presented here as an initial step toward developing a technique capable of creating a realistic environment (ambient pressures and elevated temperatures) in an electron microscope for *in situ* studies of catalytic materials on substrates.

Recently, electron energy loss spectroscopy has been demonstrated for ambient pressure *in situ* liquid studies (Jungjohann et al., 2012) and could potentially be combined with the holder described here to track the electronic states of catalyst particles and clusters at elevated pressures and temperatures while the structure and morphology are monitored with HAADF-STEM imaging. Extending these experimental capabilities further to techniques that employ high temporal resolution such as dynamic TEM (Browning et al., 2012) could potentially allow observation of transient states of catalysts while also providing the added benefit of overcoming drift due to specimen heating. The ability to couple these novel platforms for *in situ* analysis using this new environmental cell opens up a large number of possibilities to study functional nanomaterials under relevant ambient conditions.

Acknowledgments

Development of the *in situ* holder was supported by U.S. Department of Energy (DOE) NNSA-SSAA grant number DE-FG52-06NA26213 and National Institutes of Health (NIH) grant number RR025032-01. J.E. acknowledges NIH funding support from grant number 5RC1GM091755. A portion of this work was performed at the Pacific Northwest National Laboratory, which is operated by Battelle

Memorial Institute for DOE under Contract No. DE-AC05-76RL01830. A portion of this work was performed at the Lawrence Livermore National Laboratory and supported by the Office of Science, Office of Basic Energy Sciences, Division of Materials Science and Engineering of DOE under Contract No. DE-AC52-07NA27344.

References

Allard, L., Overbury, S.H., Bigelow, W.C., Katz, M.B., Nackashi, D.P. & Damiano, J. (2012). Novel MEMS-based gas-cell/heating specimen holder provides advanced imaging capabilities for *in situ* reaction studies. *Microsc Microanal* **18**, 656–666.

Baker, R.T.K. & Harris, P.S. (1972). Controlled atmosphere electron microscopy. *J Phys E Sci Instrum* **5**, 793–797.

Bergström, D., Powell, J. & Kaplan, A.F.H. (2007). Absorptance of nonferrous alloys to Nd:YLF and Nd:YAG laser light at room temperature. *Appl Opt* **46**, 1290–1301.

Boyes, E.D. & Gai, P.L. (1997). Environmental high resolution electron microscopy and applications to chemical science. *Ultramicroscopy* **67**, 219–232.

Browning, N.D., Bonds, M.A., Campbell, G.H., Evans, J.E., LaGrange, T., Jungjohann, K.L., Masiel, D.J., McKeown, J., Mehraeen, S., Reed, B.W. & Santala, M. (2012). Recent developments in dynamic transmission electron microscopy. *Curr Opin Solid St Mater Sci* **16**, 23–30.

Butler, E.P. & Hale, K.F. (1981). *Dynamic Experiments in the Electron Microscope*. Amsterdam: North-Holland Publishing Group.

Chang, L.-Y., Barnard, A.S., Gontard, L.C. & Dunin-Borkowski, R.E. (2010). Resolving the structure of active sites on platinum catalytic nanoparticles. *Nano Lett* **10**, 3073–3076.

Creemer, J.F., Helveg, S., Hoveling, G.H., Ullmann, S., Molenbroek, A.M., Sarro, P.M. & Zandbergen, H.W. (2008). Atomic-scale electron microscopy at ambient pressure. *Ultramicroscopy* **108**, 993–998.

Creemer, J.F., Helveg, S., Kooyman, P.J., Molenbroek, A.M., Zandbergen, H.W. & Sarro, P.M. (2010). A MEMS reactor for atomic-scale microscopy of nanomaterials under industrially relevant conditions. *J Microelectromech Syst* **19**(2), 254–264.

Crewe, A.V., Isaacson, M. & Johnson, D. (1969). A simple scanning electron microscope. *Rev Sci Instrum* **40**, 241.

Crewe, A.V., Wall, J. & Langmore, J. (1970). Visibility of a single atom. *Science* **168**, 1338.

Daulton, T.L., Little, B.J., Lowe, K. & Jones-Meehan, J. (2001). *In situ* environmental cell-transmission electron microscopy study of microbial reduction of chromium(VI) using electron energy loss spectroscopy. *Microsc Microanal* **7**, 470–485.

de Jonge, N., Bigelow, W.C. & Veith, G.M. (2010). Atmospheric pressure scanning transmission electron microscopy. *Nano Lett* **10**, 1028–1031.

Deshmukh, P.V., Gronsky, J.J. & Fischione, P.E. (2012). *In situ* holder assembly, U.S. Patent 8178851. Alexandria, VA: U.S. Patent and Trademark Office.

Evans, J.E., Jungjohann, K.L., Browning, N.D. & Arslan, I. (2011). Controlled growth of nanoparticles from solution with *in situ* liquid transmission electron microscopy. *Nano Lett* **11**, 2809–2813.

Gai, P.L., Boyes, E.D., Helveg, S., Hansen, P.L., Giorgio, S. & Henry, C.R. (2007). Atomic-resolution environmental transmission electron microscopy for probing gas-solid reactions in heterogeneous catalysis. *Mater Res Bull* **32**, 1044–1050.

Giorgio, S., Joao, S.S., Nitsche, S., Chaudanson, D., Sitja, G. & Henry, C.R. (2006). Environmental electron microscopy (ETEM) for catalysts with a closed E-cell with carbon windows. *Ultramicroscopy* **106**, 503–507.

Hansen, P.L., Helveg, S. & Datye, A.K. (2006). Atomic-scale imaging of supported metal nanocluster catalysts in the working state. *Adv Catal* **50**, 77–95.

Hansen, P.L., Wagner, J.B., Helveg, S., Rostrup-Nielsen, J.R., Clausen, B.S. & Topsoe, H. (2002). Atom-resolved imaging of dynamic shape changes in supported copper nanocrystals. *Science* **295**, 2053–2055.

Heide, H.G. (1962). Electron microscopic observation of specimens under controlled gas pressure. *J Cell Biol* **13**, 147–152.

Helveg, S., López-Cartes, C., Sehested, J., Hansen, P.L., Bjerne, S.C., Rostrup-Nielsen, J.R., Abild-Pederson, F. & Nørskov, J.K. (2004). Atomic-scale imaging of carbon nanofibre growth. *Nature* **427**, 426–429.

Henderson, R., Baldwin, J.M., Downing, K.H., Lepault, J. & Zemlin, F. (1986). Structure of purple membrane from halobacterium halobium: Recording, measurement and evaluation of electron micrographs at 3.5 Å resolution. *Ultramicroscopy* **19**, 147–178.

Howie, A., Marks, L.D. & Pennycook, S.J. (1982). New imaging methods for catalyst particles. *Ultramicroscopy* **8**, 163–174.

Jungjohann, K.L., Evans, J.E., Aguiar, J., Arslan, I. & Browning, N.D. (2012). Atomic-scale imaging and spectroscopy for *in situ* liquid scanning transmission electron microscopy. *Microsc Microanal* **18**, 621–627.

Komatsu, M. & Mori, H. (2005). *In situ* HVEM study on copper oxidation using an improved environmental cell. *J Electron Microsc* **54**, 99–107.

Konishi, H., Ishikawa, A., Jiang, Y.-B., Buseck, P. & Xu, H. (2003). Sealed environmental cell microscopy. *Microsc Microanal* **9**, 902–903.

Lee, T.C., Dewald, D.K., Eades, J.A., Robertson, I.M. & Birnbaum, H.K. (1991). An environmental cell transmission electron microscope. *Rev Sci Instrum* **62**, 1438–1444.

Marton, L. (1935). La microscopie electronique des objets biologiques. *Bull Classe Sci Acad Roy Belgique* **21**, 553–564.

Mkhoyan, K.A., Maccagnano-Zacher, S.E., Kirkland, E.J. & Silcox, J. (2008). Effects of amorphous layers on ADF-STEM imaging. *Ultramicroscopy* **108**, 791–803.

Nellist, P.D., Chisholm, M.F., Dellby, N., Krivanek, O.L., Murfitt, M.F., Szilagyi, Z.S., Lupini, A.R., Borisevich, A., Sides, W.H., Jr. & Pennycook, S.J. (2004). Direct sub-Angstrom imaging of a crystal lattice. *Science* **305**, 1741.

Niu, K.Y., Yang, J., Kulinich, S.A., Sun, J. & Du, X.W. (2010). Hollow nanoparticles of metal oxides and sulfides: Fast preparation via laser ablation in liquid. *Langmuir* **26**, 16652–16657.

Parkinson, G.M. (1989). High resolution, *in-situ* controlled atmosphere transmission electron microscopy (CATEM) of heterogeneous catalysts. *Catal Lett* **2**, 303–307.

Pennycook, S.J. (1981). Study of supported ruthenium catalysts by STEM. *J Microsc* **124**, 15–22.

Pennycook, S.J. (1989). Z-contrast STEM for materials science. *Ultramicroscopy* **30**, 58–69.

Pennycook, S.J., Howie, A., Shannon, M.D. & Whyman, R. (1983). Characterization of supported catalysts by high-resolution stem. *J Mol Catal* **20**, 345–355.

Robertson, I.M. & Teter, D. (1998). Controlled environmental transmission electron microscopy. *Microsc Res Techniq* **42**, 260–269.

Sharma, R. (2001). Design and applications of environmental cell transmission electron microscope for *in situ* observations of gas-solid reactions. *Microsc Microanal* **7**, 494–506.

Sharma, R. (2005). An environmental transmission electron microscope for *in situ* synthesis and characterization of nanomaterials. *J Mater Res* **20**, 1695–1707.

Sharma, R. & Weiss, K. (1998). Development of a TEM to study *in situ* structural and chemical changes at an atomic level during gas-solid interactions at elevated temperatures. *Microsc Res Techniq* **42**, 270–280.

Treacy, M.M.J., Howie, A. & Wilson, C.J. (1978). Z contrast of platinum and palladium catalysts. *Philos Mag A* **38**, 569.

Ueda, K., Kawasaki, T., Hasegawa, H., Tanji, T. & Ichihashi, M. (2008). First observation of dynamic shape changes of a gold nanoparticle catalyst under reaction gas environment by transmission electron microscopy. *Surf Interface Anal* **40**, 1725–1727.

Wang, R., Crozier, P.A. & Sharma, R. (2009). Structural transformation in ceria nanoparticles during redox processes. *J Phys Chem C* **113**, 5700–5704.

Yaguchi, T., Suzuki, M., Watabe, A., Nagakubo, Y., Ueda, K. & Kamino, T. (2011). Development of a high temperature-atmospheric pressure environmental cell for high-resolution TEM. *J Electron Microsc* **60**, 217–225.

Zhang, M., Olson, E.A., Twesten, R.D., Wen, J.G., Allen, L.H., Robertson, I.M. & Petrov, I. (2005). *In situ* transmission electron microscopy studies enabled by microelectromechanical system technology. *J Mater Res* **20**, 1802–1807.

Zingg, D.S. & Hercules, D.M. (1978). Electron spectroscopy for chemical analysis studies of lead sulfide oxidation. *J Phys Chem* **82**, 1992–1995.